The Astrophysical Journal, 1000:124 (14pp), 2026 March 20 https://doi.org/10.3847/1538-4357/ae43df

Constraints on the Correlation of IceCube Neutrinos with a Tracer of Nearby Large-scale Structure

R. Abbasi[1], M. Ackermann[2], J. Adams[3], S. K. Agarwalla[4,64], J. A. Aguilar[5], M. Ahlers[6], J.M. Alameddine[7], S. Ali[8], N. M. Amin[9], K. Andeen[10], C. Argüelles[11], Y. Ashida[12], S. Athanasiadou[2], S. N. Axani[9], R. Babu[13], X. Bai[14], J. Baines-Holmes[4], A. Balagopal V.[4,9], S. W. Barwick[15], S. Bash[16], V. Basu[12], R. Bay[17], J. J. Beatty[18,19], J. Becker Tjus[20,65], P. Behrens[21], J. Beise[22], C. Bellenghi[16], B. Benkel[2], S. BenZvi[23], D. Berley[24], E. Bernardini[25,66], D. Z. Besson[8], E. Blaufuss[24], L. Bloom[26], S. Blot[2], I. Bodo[4], F. Bontempo[27], J. Y. Book Motzkin[11], C. Boscolo Meneguolo[25,66], S. Böser[28], O. Botner[22], J. Böttcher[21], J. Braun[4], B. Brinson[29], Z. Brisson-Tsavoussis[30], R. T. Burley[31], D. Butterfield[4], M. A. Campana[32], K. Carloni[11], J. Carpio[33,34], S. Chattopadhyay[4,64], N. Chau[5], Z. Chen[35], D. Chirkin[4], S. Choi[12], B. A. Clark[24], A. Coleman[22], P. Coleman[21], G. H. Collin[36], D. A. Coloma Borja[25], A. Connolly[18,19], J. M. Conrad[36], D. F. Cowen[37,38], C. De Clercq[39], J. J. DeLaunay[37], D. Delgado[11], T. Delmeulle[5], S. Deng[21], P. Desiati[4], K. D. de Vries[39], G. de Wasseige[40], T. DeYoung[13], J. C. Díaz-Vélez[4], S. DiKerby[13], T. Ding[33,34], M. Dittmer[41], A. Domi[42], L. Draper[12], L. Dueser[21], D. Durnford[43], K. Dutta[28], M. A. DuVernois[4], T. Ehrhardt[28], L. Eidenschink[16], A. Eimer[42], P. Eller[16], E. Ellinger[44], D. Elsässer[7], R. Engel[27,45], H. Erpenbeck[4], W. Esmail[41], S. Eulig[11], J. Evans[24], P. A. Evenson[9], K. L. Fan[24], K. Fang[4], K. Farrag[46], A. R. Fazely[47], A. Fedynitch[48], N. Feigl[49], C. Finley[50], L. Fischer[2], D. Fox[37], A. Franckowiak[20], S. Fukami[2], P. Fürst[21], J. Gallagher[51], E. Ganster[21], A. Garcia[11], M. Garcia[9], G. Garg[4,64], E. Genton[11,40], L. Gerhardt[52], A. Ghadimi[26], T. Glüsenkamp[22], J. G. Gonzalez[9], S. Goswami[33,34], A. Granados[13], D. Grant[53], S. J. Gray[24], S. Griffin[4], S. Griswold[23], K. M. Groth[6], D. Guevel[4], C. Günther[21], P. Gutjahr[7], C. Ha[54], C. Haack[42], A. Hallgren[22], L. Halve[21], F. Halzen[4], L. Hamacher[21], M. Ha Minh[16], M. Handt[21], K. Hanson[4], J. Hardin[36], A. A. Harnisch[13], P. Hatch[30], A. Haungs[27], J. Häussler[21], K. Helbing[44], J. Hellrung[20], B. Henke[13], L. Hennig[42], F. Henningsen[53], L. Heuermann[21], R. Hewett[3], N. Heyer[22], S. Hickford[44], A. Hidvegi[50], C. Hill[46], G. C. Hill[31], R. Hmaid[46], K. D. Hoffman[24], D. Hooper[4], S. Hori[4], K. Hoshina[4,67], M. Hostert[11], W. Hou[27], M. Hrywniak[50], T. Huber[27], K. Hultqvist[50], K. Hymon[7,48], A. Ishihara[46], W. Iwakiri[46], M. Jacquart[6], S. Jain[4], O. Janik[42], M. Jansson[40], M. Jeong[12], M. Jin[11], N. Kamp[11], D. Kang[27], W. Kang[32], X. Kang[32], A. Kappes[41], L. Kardum[7], T. Karg[2], M. Karl[16], A. Karle[4], A. Katil[43], M. Kauer[4], J. L. Kelley[4], M. Khanal[12], A. Khatee Zathul[4], A. Kheirandish[33,34], H. Kimku[54], J. Kiryluk[35], C. Klein[42], S. R. Klein[17,52], Y. Kobayashi[46], A. Kochocki[13], R. Koirala[9], H. Kolanoski[49], T. Kontrimas[16], L. Köpke[28], C. Kopper[42], D. J. Koskinen[6], P. Koundal[9], M. Kowalski[2,49], T. Kozynets[6], A. Kravka[12], N. Krieger[20], J. Krishnamoorthi[4,64], T. Krishnan[11], K. Kruiswijk[40], E. Krupczak[13], A. Kumar[2], E. Kun[20], N. Kurahashi[32], N. Lad[2], C. Lagunas Gualda[16], L. Lallement Arnaud[5], M. Lamoureux[40], M. J. Larson[24], F. Lauber[44], J. P. Lazar[40], K. Leonard DeHolton[38], A. Leszczyńska[9], J. Liao[29], C. Lin[9], Q. R. Liu[53], Y. T. Liu[38], M. Liubarska[43], C. Love[32], L. Lu[4], F. Lucarelli[55], W. Luszczak[18,19], Y. Lyu[17,52], M. Macdonald[11], J. Madsen[4], E. Magnus[39], Y. Makino[4], E. Manao[16], S. Mancina[25,68], A. Mand[4], I. C. Mariş[5], S. Marka[56], Z. Marka[56], L. Marten[21], I. Martinez-Soler[11], R. Maruyama[57], J. Mauro[40], F. Mayhew[13], F. McNally[58], J. V. Mead[6], K. Meagher[4], S. Mechbal[2], A. Medina[19], M. Meier[46], Y. Merckx[39], L. Merten[20], J. Mitchell[47], L. Molchany[14], S. Mondal[12], T. Montaruli[55], R. W. Moore[43], Y. Morii[46], A. Mosbrugger[42], M. Moulai[4], D. Mousadi[2], E. Moyaux[40], T. Mukherjee[27], R. Naab[2], M. Nakos[4], U. Naumann[44], J. Necker[2], L. Neste[50], M. Neumann[41], H. Niederhausen[13], M. U. Nisa[13], K. Noda[46], A. Noell[21], A. Novikov[9], A. Obertacke[50], V. O'Dell[4], A. Olivas[24], R. Orsoe[16], J. Osborn[4], E. O'Sullivan[22], V. Palusova[28], H. Pandya[9], A. Parenti[5], N. Park[30], V. Parrish[13], E. N. Paudel[26], L. Paul[14], C. Pérez de los Heros[22], T. Pernice[2], T. C. Petersen[6], J. Peterson[4], M. Plum[14], A. Pontén[22], V. Poojyam[26], Y. Popovych[28], M. Prado Rodriguez[4], B. Pries[13], R. Procter- Murphy[24], G. T. Przybylski[52], L. Pyras[12], C. Raab[40], J. Rack-Helleis[28], N. Rad[2], M. Ravn[22], K. Rawlins[59], Z. Rechav[4], A. Rehman[9], I. Reistroffer[14], E. Resconi[16], S. Reusch[2], C. D. Rho[60], W. Rhode[7], L. Ricca[40], B. Riedel[4], A. Rifaie[44], E. J. Roberts[31], M. Rongen[42], A. Rosted[46], C. Rott[12], T. Ruhe[7], L. Ruohan[16], D. Ryckbosch[61], J. Saffer[45], D. Salazar-Gallegos[13], P. Sampathkumar[27], A. Sandrock[44], G. Sanger-Johnson[13], M. Santander[26], S. Sarkar[62], J. Savelberg[21], M. Scarnera[40], P. Schaile[16], M. Schaufel[21], H. Schieler[27], S. Schindler[42], L. Schlickmann[28], B. Schlüter[41], F. Schlüter[5], N. Schmeisser[44], T. Schmidt[24], F. G. Schröder[9,27], L. Schumacher[42], S. Schwirn[21], S. Sclafani[24], D. Seckel[9], L. Seen[4], M. Seikh[8], S. Seunarine[63], P. A. Sevle Myhr[40], R. Shah[32], S. Shefali[45], N. Shimizu[46], B. Skrzypek[17], R. Snihur[4], J. Soedingrekso[7], A. Sègaard[6], D. Soldin[12], P. Soldin[21], G. Sommani[20], C. Spannfellner[16], G. M. Spiczak[63], C. Spiering[2], J. Stachurska[61], M. Stamatikos[19], T. Stanev[9], T. Stezelberger[52], T. Stürwald[44], T. Stuttard[6], G. W. Sullivan[24], I. Taboada[29], S. Ter-Antonyan[47], A. Terliuk[16], A. Thakuri[14], M. Thiesmeyer[4], W. G. Thompson[11], J. Thwaites[4], S. Tilav[9], K. Tollefson[13], S. Toscano[5], D. Tosi[4], A. Trettin[2], A. K. Upadhyay[4,64], K. Upshaw[47], A. Vaidyanathan[10], N. Valtonen-Mattila[20,22], J. Valverde[10], J. Vandenbroucke[4], T. Van Eeden[2], N. van Eijndhoven[39], L. Van Rootselaar[7], J. van Santen[2], J. Vara[41], F. Varsi[45], M. Venugopal[27], M. Vereecken[40], S. Vergara Carrasco[3], S. Verpoest[9], D. Veske[56], A. Vijai[24], J. Villarreal[36], C. Walck[50], A. Wang[29],

E. H. S. Warrick[26], C. Weaver[13], P. Weigel[36], A. Weindl[27], J. Weldert[28], A. Y. Wen[11], C. Wendt[4], J. Werthebach[7], M. Weyrauch[27], N. Whitehorn[13], C. H. Wiebusch[21], D. R. Williams[26], L. Witthaus[7], M. Wolf[16], G. Wrede[42], X. W. Xu[47], J. P. Yanez[43], Y. Yao[4], E. Yildizci[4], S. Yoshida[46], R. Young[8], F. Yu[11], S. Yu[12], T. Yuan[4], A. Zander Jurowitzki[16], A. Zegarelli[20], S. Zhang[13], Z. Zhang[35], P. Zhelnin[11], and P. Zilberman[4]

IceCube Collaboration

[1] Department of Physics, Loyola University Chicago, Chicago, IL 60660, USA; analysis@icecube.wisc.edu
[2] Deutsches Elektronen-Synchrotron DESY, Platanenallee 6, D-15738 Zeuthen, Germany
[3] Department of Physics and Astronomy, University of Canterbury, Private Bag 4800, Christchurch, New Zealand
[4] Department of Physics and Wisconsin IceCube Particle Astrophysics Center, University of Wisconsin–Madison, Madison, WI 53706, USA
[5] Université Libre de Bruxelles, Science Faculty CP230, B-1050 Brussels, Belgium
[6] Niels Bohr Institute, University of Copenhagen, DK-2100 Copenhagen, Denmark
[7] Department of Physics, TU Dortmund University, D-44221 Dortmund, Germany
[8] Department of Physics and Astronomy, University of Kansas, Lawrence, KS 66045, USA
[9] Bartol Research Institute and Department of Physics and Astronomy, University of Delaware, Newark, DE 19716, USA
[10] Department of Physics, Marquette University, Milwaukee, WI 53201, USA
[11] Department of Physics and Laboratory for Particle Physics and Cosmology, Harvard University, Cambridge, MA 02138, USA
[12] Department of Physics and Astronomy, University of Utah, Salt Lake City, UT 84112, USA
[13] Department of Physics and Astronomy, Michigan State University, East Lansing, MI 48824, USA
[14] Physics Department, South Dakota School of Mines and Technology, Rapid City, SD 57701, USA
[15] Department of Physics and Astronomy, University of California, Irvine, CA 92697, USA
[16] Physik Department, Technische Universität München, D-85748 Garching, Germany
[17] Department of Physics, University of California, Berkeley, CA 94720, USA
[18] Department of Astronomy, Ohio State University, Columbus, OH 43210, USA
[19] Department of Physics and Center for Cosmology and Astro-Particle Physics, Ohio State University, Columbus, OH 43210, USA
[20] Fakultät für Physik & Astronomie, Ruhr-Universität Bochum, D-44780 Bochum, Germany
[21] III. Physikalisches Institut, RWTH Aachen University, D-52056 Aachen, Germany
[22] Department of Physics and Astronomy, Uppsala University, Box 516, SE-75120 Uppsala, Sweden
[23] Department of Physics and Astronomy, University of Rochester, Rochester, NY 14627, USA
[24] Department of Physics, University of Maryland, College Park, MD 20742, USA
[25] Dipartimento di Fisica e Astronomia Galileo Galilei, Università Degli Studi di Padova, I-35122 Padova PD, Italy
[26] Department of Physics and Astronomy, University of Alabama, Tuscaloosa, AL 35487, USA
[27] Karlsruhe Institute of Technology, Institute for Astroparticle Physics, D-76021 Karlsruhe, Germany
[28] Institute of Physics, University of Mainz, Staudinger Weg 7, D-55099 Mainz, Germany
[29] School of Physics and Center for Relativistic Astrophysics, Georgia Institute of Technology, Atlanta, GA 30332, USA
[30] Department of Physics, Engineering Physics, and Astronomy, Queen's University, Kingston, ON K7L 3N6, Canada
[31] Department of Physics, University of Adelaide, Adelaide, 5005, Australia
[32] Department of Physics, Drexel University, 3141 Chestnut Street, Philadelphia, PA 19104, USA
[33] Department of Physics & Astronomy, University of Nevada, Las Vegas, NV 89154, USA
[34] Nevada Center for Astrophysics, University of Nevada, Las Vegas, NV 89154, USA
[35] Department of Physics and Astronomy, Stony Brook University, Stony Brook, NY 11794-3800, USA
[36] Department of Physics, Massachusetts Institute of Technology, Cambridge, MA 02139, USA
[37] Department of Astronomy and Astrophysics, Pennsylvania State University, University Park, PA 16802, USA
[38] Department of Physics, Pennsylvania State University, University Park, PA 16802, USA
[39] Vrije Universiteit Brussel (VUB), Dienst ELEM, B-1050 Brussels, Belgium
[40] Centre for Cosmology, Particle Physics and Phenomenology (CP3), Université catholique de Louvain, Louvain-la-Neuve, Belgium
[41] Institut für Kernphysik, Universität Münster, D-48149 Münster, Germany
[42] Erlangen Centre for Astroparticle Physics, Friedrich-Alexander-Universität Erlangen-Nürnberg, D-91058 Erlangen, Germany
[43] Department of Physics, University of Alberta, Edmonton, Alberta, T6G 2E1, Canada
[44] Department of Physics, University of Wuppertal, D-42119 Wuppertal, Germany
[45] Karlsruhe Institute of Technology, Institute of Experimental Particle Physics, D-76021 Karlsruhe, Germany
[46] Department of Physics and The International Center for Hadron Astrophysics, Chiba University, Chiba 263-8522, Japan
[47] Department of Physics, Southern University, Baton Rouge, LA 70813, USA
[48] Institute of Physics, Academia Sinica, Taipei, 11529, Taiwan
[49] Institut für Physik, Humboldt-Universität zu Berlin, D-12489 Berlin, Germany
[50] Oskar Klein Centre and Department of Physics, Stockholm University, SE-10691 Stockholm, Sweden
[51] Department of Astronomy, University of Wisconsin–Madison, Madison, WI 53706, USA
[52] Lawrence Berkeley National Laboratory, Berkeley, CA 94720, USA
[53] Department of Physics, Simon Fraser University, Burnaby, BC V5A 1S6, Canada
[54] Department of Physics, Chung-Ang University, Seoul 06974, Republic of Korea
[55] Département de physique nucléaire et corpusculaire, Université de Genève, CH-1211 Genève, Switzerland
[56] Columbia Astrophysics and Nevis Laboratories, Columbia University, New York, NY 10027, USA
[57] Department of Physics, Yale University, New Haven, CT 06520, USA
[58] Department of Physics, Mercer University, Macon, GA 31207-0001, USA
[59] Department of Physics and Astronomy, University of Alaska Anchorage, 3211 Providence Drive, Anchorage, AK 99508, USA
[60] Department of Physics, Sungkyunkwan University, Suwon 16419, Republic of Korea
[61] Department of Physics and Astronomy, University of Gent, B-9000 Gent, Belgium

[62] Department of Physics, University of Oxford, Parks Road, Oxford OX1 3PU, UK
[63] Department of Physics, University of Wisconsin, River Falls, WI 54022, USA
Received 2025 October 20; revised 2026 February 6; accepted 2026 February 6; published 2026 March 17

Abstract

The IceCube Neutrino Observatory has observed extragalactic astrophysical neutrinos with an apparently isotropic distribution. Only a small fraction of the observed astrophysical neutrinos can be explained by known sources. Neutrino production is thought to occur in energetic environments that are ultimately powered by the gravitational collapse of dense regions of the large-scale mass distribution in the universe. Whatever their identity, neutrino sources likely trace this large-scale mass distribution. The clustering of neutrinos with a tracer of the large-scale structure may provide insight into the distribution of neutrino sources with respect to redshift and the identity of neutrino sources. We implement a two-point angular cross correlation of the Northern sky track events with an infrared galaxy catalog derived from the Wide-field Infrared Survey Explorer (WISE) and Two Micron All Sky Survey (2MASS) source catalogs, which trace the nearby large-scale structure. No statistically significant correlation is found between the neutrinos and this infrared galaxy catalog. We find that $\leqslant$54% of the diffuse muon neutrino flux can be attributed to sources correlated with the galaxy catalog with 90% confidence. Additionally, when assuming that the neutrino source comoving density evolves following a power law in redshift, $dN_s/dV \quad (1+z)^k$, we find that sources with negative evolution, in particular $k < -1.75$, are disfavored at the 90% confidence level.

Unified Astronomy Thesaurus concepts: Neutrino astronomy (1100); Two-point correlation function (1951); Extragalactic astronomy (506); Particle astrophysics (96); Large-scale structure of the universe (902)

1. Introduction

The IceCube Neutrino Observatory has observed a diffuse flux of astrophysical neutrinos with extragalactic origin (M. G. Aartsen et al. 2013, 2015, 2019, 2020a; R. Abbasi et al. 2021, 2022a, 2024). For virtually all of these extragalactic astrophysical neutrinos, their sources remain unknown. The extragalactic diffuse astrophysical neutrino flux appears isotropic; no large-scale anisotropy has been found. Point-like neutrino emission has been observed from the Seyfert galaxy NGC 1068 and the blazar TXS 0506+056 (M. G. Aartsen et al. 2018a; M. G. Aartsen et al. 2018b; R. Abbasi et al. 2022b); however, these two sources can only explain a few percent of the diffuse neutrino flux. Astrophysical neutrinos have been observed from the galactic plane (R. Abbasi et al. 2023), but they cannot account for the entire astrophysical diffuse flux.

There have been several prior studies searching for anisotropies in the IceCube neutrino data. K. Fang et al. (2020) searched for correlations of 3 years of IceCube data with infrared galaxies and placed an upper limit on the correlation. M. G. Aartsen et al. (2020b) searched for neutrino emission correlated with the large-scale structure with both $z < 0.1$ and $z < 0.03$ using the 2MASS Redshift Survey and a template-based search with 7 years of muon neutrino events. The upper limits on this neutrino emission are consistent with the observed diffuse flux. M. Negro et al. (2023) performed a two-point angular cross-correlation analysis of IceCube neutrinos with the anisotropic unresolved γ-ray background (UGRB) observed by Fermi-LAT (M. Ackermann et al. 2018). They found that less than 1% of the observed diffuse flux could be explained by the decay of pions created in energetic unresolved blazars in the Fermi-LAT γ-ray background. A. Ouellette & G. Holder (2024) performed a cross-correlation analysis across multiple redshift bins, resulting in upper limits on the correlation of IceCube neutrinos and the large-scale structure over a range of redshifts.

The two-point angular cross-correlation function is widely used in cosmology to measure the degree of clustering of two astrophysical populations (P. J. E. Peebles 1980). The two-point angular cross-power spectrum is the correlation function expressed as a weighted sum of spherical harmonics where the weights are given by the inner product of the correlation function with each spherical harmonic. The cross-power spectrum can be calculated quickly for large catalogs when pixelized, so it is computationally efficient for the analysis of millions of neutrinos with a similarly sized tracer of large-scale structure. We optimize the method of K. Fang et al. (2020) and apply the two-point angular cross-correlation function to a set of Northern sky muon neutrino candidates observed by IceCube from 2011 to 2021 and an infrared galaxy catalog.

We explain the derivation of the galaxy catalog in Section 2. We describe the IceCube data used for this analysis in Section 3 and the analysis method in Section 4. We present the results in Section 5. We discuss the results in Section 6 and conclude in Section 7.

2. UnWISE–2MASS Galaxy Catalog

The Two Micron All Sky Survey (2MASS) is a near-infrared survey performed by a pair of ground-based near-infrared telescopes located at Mount Hopkins, Arizona, and Cerro Tololo, Chile (M. F. Skrutskie et al. 2006). The telescopes observed the full sky in three filters, H, J, K_s, corresponding to central wavelengths 1.25, 1.65, and 2.16 μm. 2MASS produced an all-sky catalog containing photometry

[64] Also at the Institute of Physics, Sachivalaya Marg, Sainik School Post, Bhubaneswar 751005, India.
[65] Also at the Department of Space, Earth and Environment, Chalmers University of Technology, 412 96 Gothenburg, Sweden.
[66] Also at INFN Padova, I-35131 Padova, Italy.
[67] Also at the Earthquake Research Institute, University of Tokyo, Bunkyo, Tokyo 113-0032, Japan.
[68] Now at INFN Padova, I-35131 Padova, Italy.

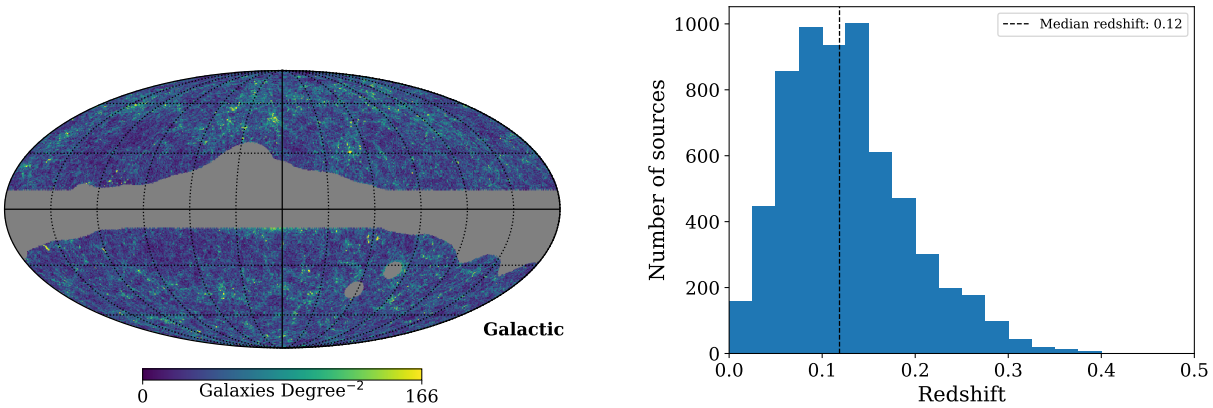

Figure 1. Left: the density of unWISE–2MASS galaxies on the sky. The gray region combines a 10° region surrounding the galactic plane and a Planck dust map. The LMC and SMC are masked as well. Right: the redshift distribution of the unWISE–2MASS catalog found by cross-matching sources with the GAMA redshift catalog. The GAMA redshifts are spectroscopically measured, so they are precise enough to neglect the statistical uncertainty. The catalog is magnitude-limited and has a tail at larger redshifts. The median redshift is 0.12, and the 10th and 90th percentiles are 0.05 and 0.22.

and astrometry for 471 million sources. The Wide-field Infrared Survey Explorer (WISE) is a far-infrared space telescope that performed a survey of the entire sky in four bands, W1, W2, W3, and W4 (E. L. Wright et al. 2010). The NEOWISE mission extends the original mission focused on near-Earth objects (A. Mainzer et al. 2011). The unWISE catalog is a reprocessing of data from the initial and extended mission, including W1 and W2 photometry from the extended mission, to create the deepest WISE catalog yet (E. F. Schlafly et al. 2019). We have produced galaxy overdensity maps (as described in Appendix A). We reproduce the method of A. Kovács & I. Szapudi (2015) to reject sources in the unWISE–2MASS catalog that are likely stellar. We also apply magnitude cuts of $W1 \leqslant 15.2$ and $J < 16.5$ to improve the spatial uniformity of the catalog. The redshift distribution of the catalog is estimated by cross-matching a subset of the unWISE–2MASS catalog with the Galaxy and Mass Assembly (GAMA) catalog (S. P. Driver et al. 2022). Despite the filtering, there is still contamination from galactic sources near the galactic plane. We apply a mask derived from the Planck dust map (developed by N. Aghanim et al. 2020) and exclude sky pixels with galactic latitude ($-10^{\circ} < b < 10^{\circ}$). The Large and Small Magellanic Clouds (LMC and SMC) are extended infrared sources that themselves contain stars that may be resolved by WISE and 2MASS. Two $0.^{\circ}5$ radius circles surrounding both the LMC and SMC are excluded. The final galaxy overdensity map and redshift distribution are shown in Figure 1. The median redshift of these sources is 0.12, and the 10% and 90% range is 0.05 to 0.22. The selection of an appropriate galaxy catalog is driven primarily by three factors: high completeness, low stellar contamination, and nearly full sky coverage. We developed an extension of the infrared catalog developed by A. Kovács & I. Szapudi (2015) and used by K. Fang et al. (2020), which satisfies these requirements. The relative importance of each of these factors is described in Section 4.

3. IceCube Data

The IceCube Neutrino Observatory is a set of 86 strings bearing 5160 digital optical modules (DOMs; K. Hanson & O. Tarasova 2006; R. Abbasi et al. 2010; M. G. Aartsen et al. 2017). These strings are installed 1.5–2.5 km below the surface of the glacial ice at the South Pole in a hexagonal array. The DOMs carry photomultiplier tubes (PMT) and electronics to power those PMTs and communicate through the strings to the surface. Neutrinos are not directly detected; instead, the Cherenkov radiation emitted by secondary particles is observed by the DOMs. The timing and intensity of the light pulse in each DOM are used to reconstruct the energy and direction of the incoming neutrino. Astrophysical muon neutrinos may produce a muon if they undergo deep inelastic scattering through the charged current channel. This muon can traverse the detector and emit a track of Cherenkov radiation. Muons may also be produced in the atmosphere by energetic cosmic rays. The Earth is a natural filter for these, so a selection of Northern sky track events maximizes the neutrino sample purity. The cosmic-ray interactions in the atmosphere also produce muon neutrinos, which cannot be distinguished from astrophysical muon neutrinos on an event-by-event basis. Based on the measured spectral shape of the diffuse muon neutrino spectrum (R. Abbasi et al. 2022a), the astrophysical sample purity is about 1.3%. Although the muon energy may be estimated, the reconstructed energy is a lower bound on the neutrino energy because some energy may be lost by the muon before entering the detector. We use a sample of Northern sky track–like events that is similar to the one used by R. Abbasi et al. (2022a), with the restriction that we only use data from the final IceCube configuration (IC 86), taken between 2011 May 13 and 2021 May 3, with an additional 3 years of full-configuration data (IC 86-2011 to IC 86-2021). This event sample contains 507,017 events. We further apply the mask described in Section 2 (shown in Figure 1) and bin the events into logarithmically spaced reconstructed energy bins centered at 1, 10, and 100 TeV, resulting in three sets composed of 338,377, 32,281, and 723 events, totaling 371,381 events with $2.5 > \log(E_{\rm reco}/{\rm GeV}) > 5.5$ in the unmasked sky.

The neutrino counts maps are pixelated using Healpix, with NSIDE equal to 128 corresponding to approximately $0.^{\circ}5$ pixel size in three logarithmically spaced reconstructed energy bins centered at 1, 10, and 100 TeV (K. M. Górski et al. 2005). Each neutrino sky map is constructed similarly to the infrared galaxy map but includes an additional weighting factor to correct the decl.-dependent and energy-dependent exposure. First, a Healpix map containing the counts $n(\boldsymbol{x})$, with $\boldsymbol{x}$ being the unit vector corresponding to a point on the celestial sphere, is constructed for each energy bin i. The weight maps $w(\boldsymbol{x})$ are designed to make a coarse estimate of the flux incident on the

detector based on the observed counts, e.g., $\phi(\boldsymbol{x}) \approx w(\boldsymbol{x})n(\boldsymbol{x})$, where $\phi(\boldsymbol{x}) = \frac{dN}{dE}$ is the flux normalization, assuming a power-law spectrum. A true estimate of the flux would require a more sophisticated unfolding of the detector response; however, this procedure produces an acceptance map that effectively removes the decl. dependence of the effective area. The weighted neutrino overdensity in reconstructed energy bin i is

$$\delta_{\nu,i}(\boldsymbol{x}) = \frac{n_i(\boldsymbol{x})\, w_i(\boldsymbol{x}) - \langle n_i\, w_i \rangle}{\langle n_i\, w_i \rangle}, \tag{1}$$

where $\langle n\, w$ is the weighted sky map averaged over unmasked pixels using the same mask as the unWISE–2MASS overdensity. As we only use overdensity maps, any overall normalization factor is removed in Equation (1).

The weight maps are created by constructing a weighted histogram of the reconstructed sine decl. ($\sin(\delta)$) of simulated events. The weights are proportional to the flux at the reconstructed energy for a power-law spectrum. We construct a Healpix map using this histogram as a lookup table for the weight at the center of the pixel. This map is blurred with a 5° Gaussian kernel to remove the discrete bands. We do not know the spectral index of the neutrino sample a priori, so we produce weight maps for an equally spaced grid of spectral indices in the range $1 \leqslant \gamma \leqslant 4$ and take the mean over the spectral index. The weight maps are not sensitive to the choice of spectral indices and account for unequal sensitivity to different parts of the sky.

4. Angular Cross Correlation

The neutrino data are composed of three populations:

1. Astrophysical neutrinos from sources correlated with the unWISE–2MASS catalog. These neutrinos are produced in sources that exist in the same redshift range as the unWISE–2MASS catalog.
2. Astrophysical neutrinos uncorrelated with the galaxy catalog. These neutrinos may come from sources uncorrelated with the large-scale structure or from outside the redshift range probed by the unWISE–2MASS catalog.
3. Atmospheric neutrinos have an anisotropic spatial distribution that is determined by the interaction of cosmic rays with the Earth's atmosphere.

We use the parameters $f_{\mathrm{corr},i}$, $f_{\mathrm{uncorr},i}$, and $f_{\mathrm{atm},i}$ to refer to the relative contributions to the overall cross correlation coming from each of the three groups. If the correlated neutrinos represent a Poisson sampling of the unWISE–2MASS galaxies, then the f parameters can be interpreted as the fraction of observed neutrinos belonging to each group. The fractions add up to 1 because they must account for all the neutrinos observed by IceCube, i.e., $f_{\mathrm{corr},i} + f_{\mathrm{uncorr},i} + f_{\mathrm{atm},i} = 1$.

K. Fang et al. (2020) showed that the power spectrum of a multicomponent population of events in reconstructed energy bin i can be decomposed additively. The two-point angular cross-power spectrum of the two overdensity fields, as defined in Appendix B, can be written as

$$C_{\ell\, i}^{g\nu} = f_{\mathrm{corr},i}\; C_{\ell\, i}^{g\nu,\,\mathrm{corr}} + f_{\mathrm{atm},i}\; C_{\ell\, i}^{g\nu,\,\mathrm{atm}}. \tag{2}$$

In this equation, we have neglected the term regarding the uncorrelated population because $\langle C_{\ell\, i}^{g\nu,\,\mathrm{uncorr}} \rangle = 0$ by default. Its contribution to the covariance is minor since the covariance matrix is dominated by the atmospheric terms, as explained in the following discussion.

Equation (2) applies to each energy bin individually. All the energy bins will be simultaneously used in a single likelihood to maximize the statistical significance, so we reparameterize Equation (2) in terms of a single correlation strength f_{corr} and spectral index γ, assuming the astrophysical events follow a power-law energy distribution,

$$C_{\ell\, i}^{g\nu} = f_{\mathrm{corr}}\; \kappa_i(\gamma)\; C_{\ell}^{gg} + f_{\mathrm{atm},i}\; C_{\ell\, i}^{g\nu,\,\mathrm{atm}}, \tag{3}$$

where $\kappa(\gamma)$ is the ratio of detector acceptance in the given energy bin ($A_i(\gamma)$) for a given spectral index divided by the acceptance across the entire energy range ($A(\gamma)$) for the same spectral index, i.e., $\kappa(\gamma) = A_i(\gamma)/A(\gamma)$ and

$$f_{\mathrm{corr}} \equiv \frac{b_\nu}{b_g} \frac{n_{\mathrm{corr}}}{n_{\mathrm{total}}}, \tag{4}$$

where b_ν and b_g are the bias factors of the unknown neutrino source population and the galaxy sample, respectively. Although tracers of large-scale structure can be used to infer the underlying matter density, they can be biased by the physics underlying their formation. N. Kaiser (1984) found that if galaxy clusters or other large-scale structure tracers formed where the underlying density is unusually large, the correlation functions are biased by a linear factor b, relative to the underlying matter correlation. The bias can be written as

$$C_{\ell}^{gg} = b_g^2\; C_{\ell}^{mm}, \tag{5}$$

$$C_{\ell\, i}^{g\nu,\,\mathrm{corr}} = b_\nu\; b_g\; C_{\ell}^{mm}, \tag{6}$$

$$C_{\ell\, i}^{\nu\nu,\,\mathrm{corr}} = b_\nu^2\; C_{\ell}^{mm}. \tag{7}$$

See Appendix B for further discussion. Their ratio, b_ν/b_g, is left as a free parameter.

If the angular power spectrum is measured using the entire sky, each multipole is statistically independent, and the observed cross-power spectra follow a multivariate normal distribution. The use of a mask, however, causes the individual multipoles in the cross-power spectrum to be coupled. We may assume that the cross-power spectra follow a multivariate Gaussian distribution and use a covariance matrix to account for mode coupling caused by the sky masking. Specifically, we define the likelihood as

$$\log(\mathcal{L}) = \sum_i -\frac{1}{2}\, \boldsymbol{x}_i^T(\boldsymbol{\theta})\, \Sigma_i^{-1}\, \boldsymbol{x}_i(\boldsymbol{\theta}) + \text{constant}, \tag{8}$$

where $\boldsymbol{\theta} = (f_{\mathrm{corr}}\, \gamma, f_{\mathrm{atm},1}, f_{\mathrm{atm},2}, f_{\mathrm{atm},3})$ are the parameters;

$$\boldsymbol{x}_i(\boldsymbol{\theta}) = C_{\ell\, i}^{g\nu} - \left(f_{\mathrm{corr}}\; \kappa_i(\gamma)\; C_{\ell\, i}^{gg} + f_{\mathrm{atm},i}\; C_{\ell\, i}^{g\nu,\,\mathrm{atm}} \right), \tag{9}$$

following Equation (3); and Σ_i^{-1} is the inverse covariance matrix.

P. Zhang & J. F. Beacom (2004) provide expressions for the uncertainty for the individual multipoles in the angular power spectra in the case where there is an uncorrelated background. Although these neglect multipole coupling, they provide a useful heuristic for galaxy catalog construction. The ideal galaxy catalog has a large sky coverage, a low background source density, a high source density, low contamination, and high completeness. The unWISE–2MASS catalog meets these requirements in regions with high galactic latitude.

Table 1
The Best-fit Parameters Found by the Likelihood Maximization Procedure

	Null Hypothesis	Test Hypothesis
TS	⋯	2.307
P-value	⋯	0.23
χ^2	1082	1077
DoF	1120	1122
$n_{\rm corr}$	⋯	4143
$f_{\rm corr}$	⋯	0.011
Spectral index	⋯	4.0†
$f_{\rm atm,1}$	1.101	1.089
$f_{\rm atm,2}$	1.012	1.122
$f_{\rm atm,3}$	0.893	0.891

Note. The right column is the test hypothesis, where some neutrinos are correlated with the large-scale structure. The left column is the null hypothesis, where $f_{\rm corr}$ is fixed to zero. The dagger (†) indicates that the best-fit parameter lies on the boundary of the allowed parameter space. The value for $n_{\rm corr}$ assumes $b_\nu = b_g$ (see Equation (4)).

Although the atmospheric neutrino production is not actually correlated with the large-scale structure, the neutrino sample exhibits spurious correlations because we are looking at a single realization of a random process, which is itself uncorrelated with the atmospheric background, on average. At small scales, $\ell > 50$, the atmospheric event distribution is smooth, so the angular correlation is zero. We include $\ell \geqslant 10$. At these large angular scales, the atmospheric events are not isotropic and will have a nonzero contribution to the cross-power spectrum. The inclusion of the $C_{\ell,i}^{g\nu,\rm atm}$ terms accounts for this anisotropic distribution of atmospheric neutrinos at low multipoles. The matrix multiplication in Equation (8) starts from a minimum multipole $\ell_{\rm min} = 10$. Compared to the previous work (K. Fang et al. 2020), including information at large scales helps optimize the sensitivity.

The test statistic (TS) is the log-likelihood ratio test where the null hypothesis is that $f_{\rm corr} = 0$ and the test hypothesis is that $f_{\rm corr} > 0$ and γ is a free parameter. Details on the construction of models for $C_{\ell\, i}^{g\nu,\,\rm atm}$, the effect of the IceCube beam function, the likelihood, the test statistic, and the systematic uncertainties are described in Appendix C.

5. Results

The analysis method was developed while keeping the R.A. coordinates blind, in order to avoid bias that could steer the development of the method toward a preferred outcome. Once the method was finalized, the analysis was performed using the true R.A. values of the events. The observed test statistic was TS = 2.307. The background test statistic distribution was numerically estimated by generating datasets containing experimental data that have uniformly random shifts in R.A. from 0 to 2π. The data are background dominated, so the "R.A. scrambling" eliminates the spatial correlations while creating plausibly realistic signal-free data. We generated 64,700 R.A.-scrambled datasets and evaluated the test statistic for each. The *p*-value (i.e., the fraction of scrambled datasets with a higher value of TS than observed for the real data) is 0.23, which is not statistically significant. The data were well-described by the maximum likelihood test hypothesis model. The χ^2 goodness of fit, defined as $\chi^2 = \sum_{i=1}^{3} \boldsymbol{x}_i^T\, \Sigma_i^{-1}\, \boldsymbol{x}_i$, was 1082 with 1120 degrees of freedom for the null hypothesis fit. For a χ^2 distribution with k degrees of freedom, the mean is k and the standard deviation is $\sqrt{2k}$. The observed goodness of fit is -0.80σ from the mean, suggesting that the null hypothesis model describes the data well. The fit parameters are shown in Table 1.

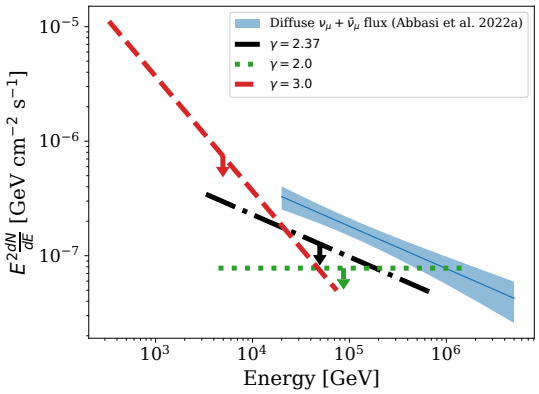

Figure 2. If the neutrinos are sampled from the unWISE–2MASS catalog, then the neutrino flux can be estimated assuming the correlation bias parameters are equal, i.e., $b_\nu = b_g$. The derived fluxes for three different spectral indices are shown in the red dashed, black dotted–dashed, and green dotted lines. The best-fit diffuse flux of muon neutrinos is shown in the blue region. If the diffuse spectral index is assumed for the correlated neutrinos, the correlated flux is less than 54% of the total diffuse flux. The cross-correlation upper limits are plotted over the 90% sensitive energy range, which is defined as the upper and lower energy range that causes the analysis sensitivity to drop by 10%.

The 90% Bayesian credible upper limit for $f_{\rm corr}$ is the value below which 90% of the posterior probability lies. The posterior is proportional to the likelihood $\mathcal{L}$ (defined through the log-likelihood in Equation (8)) multiplied by the prior; here we assume a flat prior for $f_{\rm corr}$. We evaluate the posterior probability distribution for $f_{\rm corr}$, compute its cumulative distribution function (CDF), and determine the value of $f_{\rm corr}$ such that CDF($f_{\rm corr}$) = 0.9. Practically, we calculate the CDF at evenly spaced $f_{\rm corr}$ values, fit a spline to the result, and interpolate to find the $f_{\rm corr}$ corresponding to 90% enclosed probability. When calculating an upper limit, the spectral index must be fixed. The most natural value is the observed spectral index of diffuse astrophysical muon neutrinos: $\gamma = 2.37$ (R. Abbasi et al. 2022a). We also use $\gamma = 2.0$ and $\gamma = 3.0$ as generic values that span a reasonable range consistent with diffuse astrophysical neutrino observations. The upper limits assume that $b_\nu = b_g$. The upper limits are shown in Figure 2. For $\gamma = 2.37$, less than 54% of the astrophysical diffuse muon neutrino flux at 100 TeV, as measured by R. Abbasi et al. (2022a), can be explained by sources that are correlated with the unWISE–2MASS catalog. These results depend on the assumption that neutrinos are either correlated with the unWISE–2MASS galaxies or completely uncorrelated. More sophisticated models are described in the next section.

6. Interpretation

In the previous section, we established a limit on the flux of neutrinos correlated with the large-scale structure. The limit on correlation strength may also be interpreted in terms of the evolution of the comoving neutrino source density with respect to redshift. We operate under the assumptions that the diffuse muon neutrino flux from R. Abbasi et al. (2022a) is produced by sources tracing the large-scale structure over a wide redshift range, which extends well beyond what is sampled by the

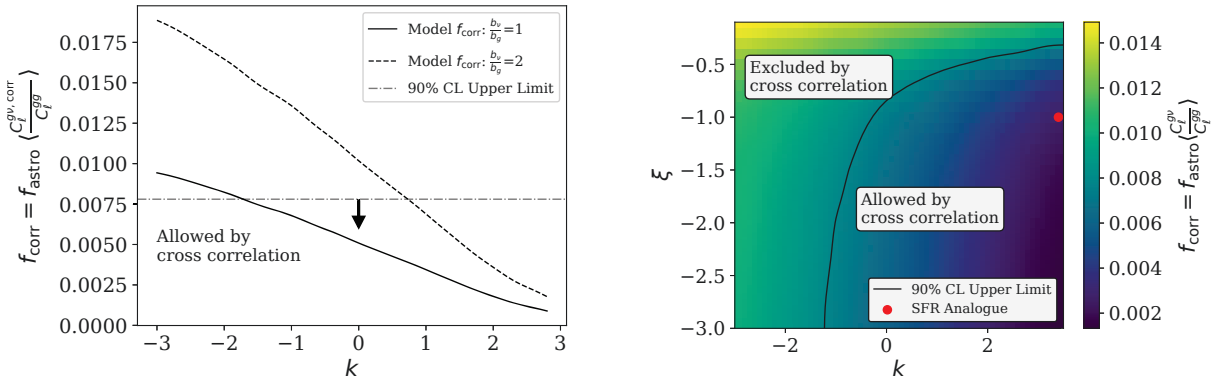

Figure 3. Left: if the neutrino sources follow a distribution of the form $\frac{dN_s}{dV} \propto (1+z)^k$, the expected correlation strength $f_{\rm corr}$ can be calculated given the ratio of diffuse astrophysical neutrinos to total neutrinos $f_{\rm astro}$. The expected correlation strength for equal bias parameters (solid black) and $\frac{b_\nu}{b_g} = 2$ (dashed line) are shown. The latter case is a pessimistic model, given that neutrino sources may form within the same dark matter halos as the unWISE–2MASS galaxies. The actual upper limit is shown by the gray dashed–dotted line. The area below the line is allowed by the upper limit. Right: if the neutrino sources follow a distribution of the form $\frac{dN_s}{dV} = (1+z)^k\, e^{z/\xi}$, and the astrophysical spectral index and sample purity are equal to the best-fit diffuse muon neutrino flux ($\gamma = 2.37$ and $f_{\rm astro} = 0.013$), the expected correlation strength can be calculated numerically using the Core Cosmology Library software. The expected correlation strength $f_{\rm corr}$ for equal bias parameters is shown in solid black. The region on the lower right predicts correlations that are weaker than the observed upper limit. For $\xi \ll 1$, the limit on power-law index approaches $k \gtrsim -1.75$, which suggests a median observed neutrino redshift $z > 0.2$. For reference, the evolution model most similar to the star formation rate model is shown as a red dot with $k = 3.4$ and $\xi = -1$.

unWISE–2MASS catalog, and that there is a single dominant neutrino source population. The comoving density of these sources can be written as $dN_s(z)/dV$. For a model of the comoving density, we compute the expected $f_{\rm corr}$ and compare this with the upper limit obtained in this work, assuming the neutrino spectral energy distribution is the same as the diffuse muon neutrino result, $\gamma = 2.37$. The calculation is done by (1) generating a Monte Carlo simulated neutrino source population, (2) calculating the neutrino flux from each source as seen from Earth, (3) constructing the distribution of neutrino flux with respect to redshift dN_ν/dz, (4) calculating the expected cross-power spectrum, and (5) calculating the expected $f_{\rm corr}$. Appendix D describes the process in detail. This approach is similar to the one used by A. Ouellette & G. Holder (2024), with an additional final step that allows us to compare with our parameterization.

Several interesting neutrino source population models can be tested with this framework, including the following:

1. Power law: $\frac{dN_s}{dV} \propto (1+z)^k$
2. Power law with cutoff: $\frac{dN_s}{dV} \propto (1+z)^k\, e^{z/\xi}$
3. Sources tracing unWISE–2MASS: $\frac{dN_s}{dV} \propto \frac{dN_g}{dV}$
4. Counts tracing unWISE–2MASS: $\frac{dN_\nu}{dV} \propto \frac{dN_g}{dV}$
5. Sources tracing the star formation rate (SFR): $\frac{dN_s}{dV} \propto \mathrm{SFR}(z)$
6. Constant comoving density: $\frac{dN_s}{dV} \propto$ constant

Power-law model. The constraints on the power-law neutrino source population are shown in Figure 3. We calculated the expected correlation strength for a variety of source-evolution power-law indices. Assuming equal bias parameters, we find $k > -1.75$ at 90% confidence.

Power law with cutoff model. Qualitatively, this model is similar to the behavior of the star formation rate, which peaks around $z = 2$. The jointly allowed parameter space of k and ξ is shown in Figure 3. The region in the bottom-right section of the figure shows the allowed values of the exponentially cutoff power-law source distribution. Below $\xi = -1$, the allowed values of k are not significantly affected. Source distributions with $\xi > -0.5$ have a higher concentration of nearby sources, so the correlation strength is inconsistent with the observed correlation upper limit.

Table 2
The Expected Correlation Strength, as Tabulated for Various Models

Model	$f_{\rm corr,model}$	$\frac{f_{\rm corr,model}}{f_{\rm corr,UL}}$
Sources tracing unWISE–2MASS	0.016	2.051
Counts tracing unWISE–2MASS	0.014	1.846
Star formation rate	0.002	0.269
Constant comoving density	0.005	0.667

Note. We disfavor models where all the sources have the same distribution with respect to redshift as the unWISE–2MASS catalog or the neutrino counts themselves follow the unWISE–2MASS. We cannot rule out models where neutrino sources follow the star formation rate, or where the neutrino sources have a uniform comoving density, unless the neutrino sources have a large bias parameter.

Additional models. The two models presented here contain free parameters that can be used to tune the correlation strength until it is consistent with the observed upper limit. The following models have no free parameters other than b_g and b_ν, so we simply present the model prediction, which can be compared to the upper limit. The model correlation strengths are summarized in Table 2. If neutrino sources trace the same redshift distribution as the unWISE–2MASS galaxies, or the neutrino sources are a subset of unWISE–2MASS sources, the correlation strength is expected to be 0.016 or approximately twice the upper limit correlation. Similarly, if the counts follow the same distribution as the unWISE–2MASS sources, the correlation strength is 0.014 or 1.8 times the upper limit. In either case, these are not consistent with the correlation nondetection. A neutrino source population that traces the star formation rate produces a much weaker correlation. The expected value is 0.002, which is approximately a quarter of the upper limit. Similarly, a neutrino source population that

has a constant comoving density produces a correlation of 0.005, which is two-thirds of the upper limit.

The star formation rate is often approximated as a power law at small redshift and starts to decrease above $z > 2$ (P. Madau & M. Dickinson 2014). This behavior can be approximated by a power law with an exponential cutoff, with $\frac{dN_s}{dV} \propto (1+z)^{3.4}\, e^{-z}$. Figure 3, right panel, shows this approximation in the context of the power law with an exponential cutoff parameter space. This model predicts $f_{\rm corr} = 0.003$. The difference is likely due to model differences at larger redshifts. The star formation rate analog is not near the detectability frontier in Figure 3, suggesting that uncertainty in the true star formation rate or small differences in the neutrino and star formation rate evolution would not affect the conclusion about the star formation rate model.

7. Conclusion

We searched for the two-point angular cross correlation of 10 years of Northern sky IceCube muon neutrinos with an infrared galaxy catalog derived from WISE and 2MASS observations. The model for the astrophysical correlated events and atmospheric background was calculated using a forward-modeling approach, which included the effect of masking and the IceCube point-spread function. The full covariance matrix was included to account for mode coupling induced by the mask. We maximized the likelihood of the overall correlation strength and power-law spectral index across the entire energy range and the atmospheric background contribution in each reconstructed energy bin. In the null hypothesis fit, we fit only the atmospheric background strength. The maximum likelihood estimation yielded a test statistic of 2.307 corresponding to a significance of 1.21σ. This is not a statistically significant result, so we placed upper limits on the correlation strength, assuming several spectral indices. Using the spectral index of the diffuse muon neutrino measurement proposed by R. Abbasi et al. (2022a), if we assume that the bias parameters are equal ($b_\nu = b_g$), and that the neutrinos are sampled from the same distribution as the unWISE–2MASS, the correlated flux is less than 54% of the diffuse flux at 100 TeV.

We can also constrain the distribution of neutrino sources with respect to redshift by estimating the expected correlation strength under a model of neutrino source distribution with respect to redshift. As a baseline, we select an $(1+z)^k$ comoving density and compute the expected correlation strength for various values of k. These model predictions are compared with the upper limit on correlation strength, assuming the diffuse muon neutrino spectral index. The upper limits disfavor models with $k \leqslant -1.75$. We also tested an exponentially cutoff comoving density $(1+z)^k e^{z/\xi}$ and placed limits on the allowed parameter space. Astrophysical neutrino production is often thought to trace the star formation rate. Such a model is consistent with the upper limit on correlation strength, as are models of uniform comoving density, as long as the neutrino source bias parameters are not exceptionally large. We disfavor models where the entire diffuse neutrino population traces the unWISE–2MASS catalog, as well as models where the neutrino counts follow the unWISE–2MASS catalog.

Future neutrino observatories with an improved angular reconstruction and additional data will allow for better measurements of the anisotropies present within the diffuse neutrino flux. In addition, discovering the origin of the diffuse muon neutrinos could be facilitated by tomographic cross-correlation studies, where the cross correlation is performed with multiple tracers spanning a large redshift range to directly reveal the neutrino source evolution with respect to redshift. A. Ouellette & G. Holder (2024) performed such a study; however, their restricted use of multipoles $\ell \geqslant 50$ limits the sensitivity in this work. A tomographic cross correlation in the style of A. Paopiamsap et al. (2024) with catalogs that include redshift information, such as the 2MASS Photometric Redshift Catalog (M. Bilicki et al. 2013) or the WISE x SuperCOSMOS Photometric Redshift Catalog (M. Bilicki et al. 2016), has the potential to reveal the redshift dependence of neutrino sources and provide insight into their identities.

Acknowledgments

The IceCube collaboration acknowledges David Guevel's significant contributions to this manuscript. The authors gratefully acknowledge support from the following agencies and institutions. United States: U.S. National Science Foundation, Office of Polar Programs; U.S. National Science Foundation, Physics Division; U.S. National Science Foundation, Established Program to Stimulate Competitive Research (EPSCoR); U.S. National Science Foundation, Office of Advanced Cyberinfrastructure; Wisconsin Alumni Research Foundation; Center for High Throughput Computing (CHTC) at the University of Wisconsin–Madison; Open Science Grid (OSG); Partnership to Advance Throughput Computing (PATh); Advanced Cyberinfrastructure Coordination Ecosystem: Services & Support (ACCESS); Frontera and Ranch Computing Project at the Texas Advanced Computing Center; U.S. Department of Energy, National Energy Research Scientific Computing Center; Particle Astrophysics Research Computing Center at the University of Maryland; Institute for Cyber-Enabled Research at Michigan State University; Astroparticle Physics Computational Facility at Marquette University; NVIDIA Corporation; and Google Cloud Platform. Belgium: Funds for Scientific Research (Fonds de la Recherche Scientifique [FNRS] and Flanders [FWO]), FWO Odysseus and Big Science Programmes, and Belgian Federal Science Policy Office (Belspo). Germany: Bundesministerium für Bildung und Forschung (BMBF), Deutsche Forschungsgemeinschaft (DFG), Helmholtz Alliance for Astroparticle Physics (HAP), Initiative and Networking Fund of the Helmholtz Association, Deutsches Elektronen Synchrotron (DESY), and the High Performance Computing cluster at RWTH Aachen University. Sweden: Swedish Research Council, Swedish Polar Research Secretariat, Swedish National Infrastructure for Computing (SNIC), and Knut and Alice Wallenberg Foundation. European Union: EGI Advanced Computing Services for Research. Australia: Australian Research Council. Canada: Natural Sciences and Engineering Research Council of Canada, Calcul Québec, Compute Ontario, Canada Foundation for Innovation, WestGrid, and Digital Research Alliance of Canada. Denmark: Villum Fonden, Carlsberg Foundation, and European Commission. New Zealand: Marsden Fund. Japan: Japan Society for Promotion of Science (JSPS) and Institute for Global Prominent Research (IGPR) of Chiba University. Korea: National Research Foundation of Korea (NRF). Switzerland: Swiss National Science Foundation (SNSF).

Appendix A
UnWISE–2MASS Catalog Map Production

Both the WISE and 2MASS point source catalogs contain galactic and extragalactic sources; the galactic sources must be removed to produce a pure large-scale structure tracer. A. Kovács & I. Szapudi (2015) identify a simple strategy based on color and magnitude cuts that discriminate between galaxies and stars. The authors use the WISE source cross-matching provided with the WISE catalog to obtain J magnitudes for the WISE sources and then exclude sources with $W1 - J > -1.7$. We also require sources to have $W1 \leqslant 15.2$ and $J < 16.5$ to improve the spatial uniformity of the catalog. Even with these cuts, the stellar contamination near the galactic plane remains high, so the authors apply a galactic plane mask derived from dust emission (based on D. J. Schlegel et al. 1998). The authors estimate the completeness of the catalog by identifying a subset of sources with spectroscopically confirmed classifications as galaxies or stars.

The authors find that the catalog contains 70% of the spectroscopically confirmed galaxies with only 1.2% contamination by stars. We reproduce these steps to produce an updated catalog using the additional WISE data in the unWISE catalog. We cross-match the unWISE sources with the 2MASS Point Source Catalog with a maximum tolerance of 3 . The resulting galaxy catalog contains 2.4 million sources distributed across 21,200 square degrees, or 51% of the sky. The distribution of unWISE–2MASS galaxies is shown in Figure 1. Despite the filtering, there is still contamination by galactic sources near the galactic plane. The galactic plane is masked using a mask derived from the Planck dust map (N. Aghanim et al. 2020) while excluding the sky pixels with galactic latitude ($-10° < b < 10°$). The LMC and SMC are extended infrared sources that themselves contain stars that may be resolved by WISE and 2MASS. Two $0.^{\circ}5$ radius circles surrounding both the LMC and SMC are excluded. The unWISE–2MASS catalog is pixelated to a Healpix map in equatorial coordinates with NSIDE equal to 128. This degree of pixelation corresponds to approximately a $0.^{\circ}5$ pixel size. The IceCube point-spread function has a full-width half-max greater than this, so there is no benefit to finer pixelation. We construct a galaxy overdensity map, defined as

$$\delta_g(\boldsymbol{x}) = \frac{n(\boldsymbol{x}) - \langle n \rangle}{\langle n \rangle}, \tag{A1}$$

where $\langle n$ is the average over the unmasked pixels and $\boldsymbol{x}$ is a unit vector.

We estimate the redshift distribution of the galaxies by cross-matching the unWISE–2MASS catalog with another galaxy catalog featuring spectroscopically measured redshifts. The GAMA survey (S. P. Driver et al. 2022) contains spectroscopic redshifts for galaxies spanning approximately 250 square degrees. For each source in the unWISE–2MASS catalog, we search for a GAMA source within 3 . If there is one, we assign the GAMA source's redshift to the unWISE–2MASS source. We find 6349 likely matches. The distribution of these redshifts is shown in Figure 1.

Appendix B
Cross-power Spectrum and Bias Factors

The two-point angular cross-power spectrum of two overdensity fields is defined by

$$C_{\ell\, i}^{g\nu} = \frac{4\pi}{2\ell + 1} \int d\cos(\theta)\, \langle \delta_g(\boldsymbol{x})\, \delta_{\nu,i}(\boldsymbol{x}') \rangle\, P_\ell^*(\cos(\theta)), \tag{B1}$$

where $\cos(\theta) = \boldsymbol{x} \cdot \boldsymbol{x}'$ for unit vectors $\boldsymbol{x}$ and $\boldsymbol{x}'$, $P_\ell^*(\cos(\theta))$ are Legendre polynomials, and the angular brackets indicate the average over field configurations. If $C_{\ell\, i}^{g\nu}$ is greater than zero, there is some common anisotropy shared by the overdensity fields at an angular scale ℓ. The overdensity maps for galaxies or neutrinos can be represented by a decomposition into multipoles

$$\delta(\boldsymbol{x}) = \sum_{\ell=0}^{\infty} \sum_{m=-\ell}^{\ell} a_{\ell m} Y_{\ell m}(\boldsymbol{x}). \tag{B2}$$

The estimator for the cross-power spectrum over a partially masked sky given the spherical harmonic decomposition is

$$C_{\ell\, i}^{g\nu} = \frac{1}{(2\ell + 1) f_{\rm sky}} \sum_{\ell=-m}^{m} a_{\ell m}^{g*} a_{\ell m, i}^{\nu}. \tag{B3}$$

The bias factors b_ν and b_g describe how strongly clustered the large-scale structure tracers are relative to the underlying matter density. The clustering is influenced by the particular physics of the formation of the tracer. At large scales, the bias parameters are linearly proportional to the angular power spectrum of the matter density. These factors can be written as

$$C_\ell^{gg} = b_g^2\, C_\ell^{mm}, \tag{B4}$$

$$C_{\ell\, i}^{g\nu,\,\rm corr} = b_\nu\, b_g\, C_\ell^{mm}, \tag{B5}$$

$$C_{\ell\, i}^{\nu\nu,\,\rm corr} = b_\nu^2\, C_\ell^{mm}. \tag{B6}$$

Substituting Equation (B4) into Equation (B5) finds that

$$C_{\ell\, i}^{g\nu,\,\rm corr} = \frac{b_\nu}{b_g} C_\ell^{gg}. \tag{B7}$$

We assume that the bias factors do not depend on neutrino energy, so that Equations (B4) and (B5) remain true for any energy-binning scheme. The values of the bias parameters depend on the physics of the tracer formation, but their values are typically $\mathcal{O}(1)$. Usually the bias factors can be estimated by comparing the autocorrelation with simulations of the underlying matter density; however, the neutrino autocorrelation is too noisy to do this because of the low astrophysical sample purity.

Appendix C
Details of Statistical Analysis

Equation (3) describes the true cross-power spectrum; however, the finite beam size and partial sky visibility must be accounted for. We adopt a forward-modeling approach in the statistical evaluation of the cross-power spectrum; thus all the cross-power spectra noted here refer to the *observed* quantities, which are modulated by the point-spread function and mask rather than the *true* quantities.

The mapping between the true cross-power spectrum and the observed cross-power spectrum would typically be described by $C_\ell^{g\nu,\rm corr} = B_\ell^g\, B_\ell^\nu\, C_\ell^{g\nu,\rm true}$f, where B_ℓ^g and B_ℓ^ν are

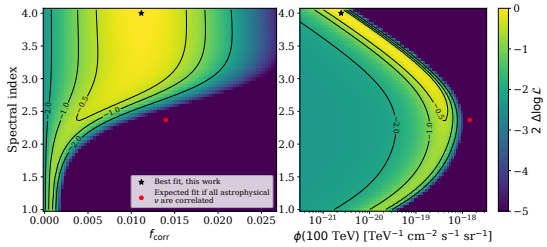

Figure C1. Left: the change in likelihood relative to the maximum likelihood value for the two astrophysical parameters is shown in color and with contours. The maximum likelihood value is on the boundary with $\gamma = 4.0$. The test statistic is not statistically significant for the maximum likelihood parameter values. The expected value of $f_{\rm corr}$ is given if all of the astrophysical neutrinos were correlated with the unWISE–2MASS catalog, assuming the spectral index is the same as the diffuse measurement (R. Abbasi et al. 2022a). Right: the same likelihood is shown in terms of the differential flux at 100 TeV.

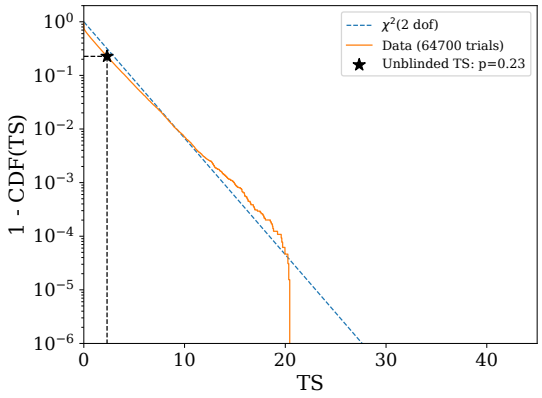

Figure C2. The TS distribution for RA-scrambled synthetic datasets. The blue dotted line shows a χ^2 distribution with 2 degrees of freedom. The unblinded TS is shown as a black star. The unblinded TS is 2.307, which is not statistically significant.

the beam functions of the galaxy and neutrino maps. This is only true if the instrument point-spread function is radially symmetric about the source and the same in every direction; neither of these conditions are met by IceCube. We directly estimate the observed $C_\ell^{g\nu,\,\rm corr}$ in each energy bin through Monte Carlo simulation. We use detailed simulations of the detector response to an impulse flux, which can be reweighted to match whatever spatial distribution and energy spectrum are desired. We use these simulations to construct 1000 purely astrophysical neutrino datasets, which are Poisson sampled from the unWISE–2MASS template, including the effects of the point-spread function and sky pixelation. In these simulations, we use a neutrino energy spectrum following a power law with an index equal to 2.5. The choice of energy spectral index in the model construction has a negligible effect.

A model for the atmospheric contribution to the cross correlation $C_\ell^{g\nu,\,\rm atm}$ is also necessary. The atmospheric model in each bin is generated in a similar way as the signal model; however, it is generated in two ways to serve as a cross-check on the consistency of the model. The first exploits the fact that the IceCube data is background dominated. The data are binned in equal-sized bins of sine decl., and a Gaussian kernel density estimate is constructed to form a continuous function as a function of decl. The value of this function of decl. is then applied to every pixel in a Healpix map, and that map is cross-correlated with the unWISE–2MASS map. The resulting cross-spectrum is used as a template for the atmospheric neutrino contribution to the total power spectrum. The aggregation of data over sine decl. almost completely destroys the spatial correlation in the data while reducing exposure to detector systematic uncertainty. In our second approach, the model was estimated using Monte Carlo data. Simulated atmospheric background events were generated and processed following the same kernel density estimation procedure. The differences between the models were negligible, suggesting that the systematic difference between these models is small.

The cross-power spectra are normally distributed as written in Equation (8). Ideally, each multipole in the cross-power spectrum is distributed independently; however, using a mask creates correlations between the multipoles. Because the data is dominated by atmospheric events, the covariance matrix is estimated by creating 64,700 sets of atmospheric-only data. The cross-power spectra are computed for each energy bin in each trial, and a covariance matrix, $\Sigma_{i,\ell_1\ell_2} = {\rm Cov}[C_{\ell_1 i}^{g\nu}, C_{\ell_2 i}^{g\nu}]$, is constructed for each energy bin from these pseudotrial power spectra. Energy bins are assumed to be independent: ${\rm Cov}[C_{\ell_1 i}^{g\nu}, C_{\ell_2 j}^{g\nu}] = 0$ for $i \quad j$. The change in likelihood for different parameter values is shown in Figure C1.

Table C1
Systematic Variations in These Parameters Were Considered while Estimating Systematic Uncertainty in the Fit Results

Systematic Varied	Value	Description
DOM Efficiency	10%	Ratio observed and simulated DOM photoelectrons
Hole Ice P0	1	Hole ice scattering parameter
Ice scattering	5%	Scattering of photons in ice
Ice absorption	5%	Scattering of photons in ice

We evaluate the statistical significance using a log-likelihood ratio test. The null hypothesis is that the data sample does not contain a population of neutrinos correlated with the unWISE–2MASS galaxies, $f_{\rm corr} = 0$, and the test hypothesis is that $f_{\rm corr} > 0$. The test statistic can be written as

$$\begin{aligned} {\rm TS} = 2(&\log(\mathcal{L}(\hat{f}_{\rm corr}, \hat{\gamma}, \hat{f}_{{\rm atm},1}, \hat{f}_{{\rm atm},2}, \hat{f}_{{\rm atm},3}) \\ &- \log(\mathcal{L}(0, \hat{\gamma}, \hat{f}_{{\rm atm},1}, \hat{f}_{{\rm atm},2}, \hat{f}_{{\rm atm},3})), \end{aligned} \tag{C1}$$

where the likelihoods in the numerator and denominator are independently maximized with respect to the parameters. Although these are nested hypotheses, we constrain the $f_{\rm corr}$ to be greater than or equal to zero. The null hypothesis lies on the boundary of the test hypothesis, so Wilk's theorem cannot be used to estimate the null hypothesis test statistic distribution. We numerically estimate the null hypothesis test statistic distribution by simulating 64,700 pseudotrials with atmospheric neutrinos and computing the test statistic for each pseudotrial. The resulting test statistic distribution resembles a χ^2 distribution with 2 degrees of freedom; however, half of the trials have TS = 0. This numerical test statistic distribution is used to evaluate the statistical significance of the likelihood ratio. The test statistic distribution is shown in Figure C2.

Systematic uncertainty arises from various unmodeled or mismodeled effects that can impact the inference process. Often, systematic uncertainty can be mitigated using data-driven methods. For example, the atmospheric model used in the cross correlation has been compared with an atmospheric

model generated using simulated events. The resulting models are consistent with the expected statistical uncertainty of the cross correlation. The systematic effect of the detector calibration on the entire analysis pipeline was evaluated using simulated datasets. The simulated datasets were created with the nominal simulated dataset, and the fit was performed with models generated with simulated datasets where detector configuration and ice properties varied. We varied the DOM efficiency (10%), hole ice scattering, ice scattering (5%), and ice absorption (5%). The systematic parameters that are varied are summarized in Table C1. A total of two tests were run. The first used simulated datasets with only atmospheric neutrinos. The second used a realistic level of signal injection, about 2500 correlated neutrinos. The systematic uncertainty is defined as $\sigma_{f,\mathrm{sys}} = \max_i(|f_i - f_{\mathrm{nominal}}|)$ and $\sigma_{\gamma,\mathrm{sys}} = \max(|\gamma_i - \gamma_{\mathrm{nominal}}|)$, where i indexes the set of Monte Carlo systematic datasets. The average fractional systematic uncertainty on the correlation strength is approximately 20%, and the average fractional systematic uncertainty on the spectral index is approximately 5%.

Appendix D
Cross-correlation Modeling

For each of the models listed in Section 6, we generate ensembles of neutrino sources using the FIRst Extragalactic Simulation Of Neutrinos and Gamma-rays (FIRESONG; C. F. Tung et al. 2021). FIRESONG is a Python code designed to simulate realistic neutrino source distributions and calculate the fluxes of those individual neutrino sources as seen on Earth. FIRESONG constructs a probability density with respect to redshift, taking into account cosmological evolution and the evolution of the source population with respect to redshift. This probability density is sampled, and the number of samples is fixed such that the expected flux from all the sources is equal to the observed diffuse muon neutrino flux. The flux of individual sources includes the effects of intrinsic luminosity functions, power-law spectra, the cosmological dimming that causes high-energy events to redshift out of the IceCube sensitive energy range, and the luminosity distance. The flux from a neutrino source with luminosity L and redshift z is $F = \frac{L}{D_L^2(1+z)^\gamma}$, where D_L is the luminosity distance and the additional factor accounts for the cosmological redshift of a power-law spectrum. Although FIRESONG produces fluxes, the cross correlation is calculated using neutrino counts. The count rate observed from an individual source is linearly proportional to the flux observed from that source, so the distribution of flux with respect to redshift is the same as the distribution of the observed counts with respect to redshift after normalizing the distributions. The weighting applied to the neutrino overdensity maps ensures that the spatially dependent effective area has a minimal effect.

After constructing a model for the distribution of neutrino flux $\frac{d\phi}{dz}$ (or equivalently counts $\frac{dN_\nu}{dz}$) as a function of redshift, we use the Core Cosmology Library (CCL) to model the cross-power spectrum (N. E. Chisari et al. 2019). The cross-correlation strength due to astrophysical neutrinos is

$$C_\ell^{g\nu,\,\mathrm{corr}} = b_g\, b_\nu \int d\chi\, \chi^{-2}\, \lambda_\nu(\chi)\, \lambda_g(\chi)\, P_k\left(\frac{\ell + \frac{1}{2}}{\chi}\right), \quad \text{(D1)}$$

where $\lambda_g = \frac{1}{N_g}\frac{dN_g}{dz(\chi)}$, N_g is the number of sources in the galaxy catalog, $\lambda_\nu = \frac{1}{N_\nu}\frac{dN_\nu}{dz(\chi)}$ is the distribution of neutrino counts, χ is the comoving distance, and P_k is the matter-density power spectrum. Similarly, the galaxy autocorrelation can be written as

$$C_\ell^{gg} = b_g^2 \int d\chi\, \chi^{-2}\, \lambda_g(\chi)^2\, P_k\left(\frac{\ell + \frac{1}{2}}{\chi}\right). \quad \text{(D2)}$$

The galaxy distribution λ_g has been obtained by cross-matching a subset of the unWISE–2MASS catalog with the GAMA spectroscopic survey. This distribution is shown in Figure 1. CCL is used to evaluate the integrals in Equations (D1) and (D2).

As we have defined the likelihood and Equation (B7), the correlation strength f_{corr} is equivalent to the ratio of the cross-power spectra and galaxy autocorrelation averaged over multipoles:

$$f_{\mathrm{corr}} = \frac{n_{\mathrm{corr}}}{n_{\mathrm{total}}}\frac{b_\nu}{b_g} \approx f_{\mathrm{astro}} \left\langle \frac{C_\ell^{g\nu,\,\mathrm{corr}}}{C_\ell^{gg}} \right\rangle. \quad \text{(D3)}$$

Inspection of Equations (D1) and (D2) shows the equality on the left occurs exactly when $\lambda_g = \lambda_\nu$. This remains approximately true as long as the redshift range of the galaxy catalog is not too large. We have numerically verified that the ratio of the cross-power spectrum and galaxy autocorrelation vary only by a few percent, dependent on multipole ℓ. The factor f_{astro} here represents the astrophysical sample purity for all neutrinos, regardless of energy. This factor can be estimated via the best-fit diffuse muon neutrino single power-law parameters using only the events with reconstructed energy in the range considered in this analysis. In this case, $f_{\mathrm{astro}} = \frac{n_{\mathrm{astro}}}{n_{\mathrm{total}}} = 0.013$.

ORCID iDs

R. Abbasi https://orcid.org/0000-0001-6141-4205
M. Ackermann https://orcid.org/0000-0001-8952-588X
S. K. Agarwalla https://orcid.org/0000-0002-9714-8866
J. A. Aguilar https://orcid.org/0000-0003-2252-9514
M. Ahlers https://orcid.org/0000-0003-0709-5631
J.M. Alameddine https://orcid.org/0000-0002-9534-9189
S. Ali https://orcid.org/0009-0001-2444-4162
K. Andeen https://orcid.org/0000-0001-9394-0007
C. Argüelles https://orcid.org/0000-0003-4186-4182
S. N. Axani https://orcid.org/0000-0001-8866-3826
X. Bai https://orcid.org/0000-0002-1827-9121
A. Balagopal V. https://orcid.org/0000-0001-5367-8876
S. W. Barwick https://orcid.org/0000-0003-2050-6714
V. Basu https://orcid.org/0000-0002-9528-2009
J. J. Beatty https://orcid.org/0000-0003-0481-4952
J. Becker Tjus https://orcid.org/0000-0002-1748-7367
J. Beise https://orcid.org/0000-0002-7448-4189
C. Bellenghi https://orcid.org/0000-0001-8525-7515
S. BenZvi https://orcid.org/0000-0001-5537-4710
E. Bernardini https://orcid.org/0000-0003-3108-1141
E. Blaufuss https://orcid.org/0000-0001-5450-1757
L. Bloom https://orcid.org/0009-0005-9938-3164
S. Blot https://orcid.org/0000-0003-1089-3001

J. Y. Book Motzkin https://orcid.org/0000-0001-6687-5959
C. Boscolo Meneguolo https://orcid.org/0000-0001-8325-4329
S. Böser https://orcid.org/0000-0002-5918-4890
O. Botner https://orcid.org/0000-0001-8588-7306
J. Böttcher https://orcid.org/0000-0002-3387-4236
B. Brinson https://orcid.org/0000-0001-9128-1159
M. A. Campana https://orcid.org/0000-0003-4162-5739
K. Carloni https://orcid.org/0000-0003-3859-3748
J. Carpio https://orcid.org/0000-0003-0667-6557
S. Chattopadhyay https://orcid.org/0009-0006-1352-2248
D. Chirkin https://orcid.org/0000-0003-4911-1345
B. A. Clark https://orcid.org/0000-0003-4089-2245
A. Coleman https://orcid.org/0000-0003-1510-1712
D. A. Coloma Borja https://orcid.org/0000-0003-0007-5793
J. M. Conrad https://orcid.org/0000-0002-6393-0438
D. F. Cowen https://orcid.org/0000-0003-4738-0787
C. De Clercq https://orcid.org/0000-0001-5266-7059
J. J. DeLaunay https://orcid.org/0000-0001-5229-1995
D. Delgado https://orcid.org/0000-0002-4306-8828
P. Desiati https://orcid.org/0000-0001-9768-1858
K. D. de Vries https://orcid.org/0000-0002-9842-4068
G. de Wasseige https://orcid.org/0000-0002-1010-5100
T. DeYoung https://orcid.org/0000-0003-4873-3783
J. C. Díaz-Vélez https://orcid.org/0000-0002-0087-0693
S. DiKerby https://orcid.org/0000-0003-2633-2196
D. Durnford https://orcid.org/0000-0002-6608-7650
M. A. DuVernois https://orcid.org/0000-0002-2987-9691
A. Eimer https://orcid.org/0009-0002-6308-0258
P. Eller https://orcid.org/0000-0001-6354-5209
D. Elsässer https://orcid.org/0000-0001-6796-3205
H. Erpenbeck https://orcid.org/0000-0001-6319-2108
W. Esmail https://orcid.org/0000-0002-0097-3668
P. A. Evenson https://orcid.org/0000-0001-7929-810X
A. R. Fazely https://orcid.org/0000-0002-6907-8020
A. Fedynitch https://orcid.org/0000-0003-2837-3477
C. Finley https://orcid.org/0000-0003-3350-390X
L. Fischer https://orcid.org/0000-0002-7645-8048
D. Fox https://orcid.org/0000-0002-3714-672X
A. Franckowiak https://orcid.org/0000-0002-5605-2219
P. Fürst https://orcid.org/0000-0002-7951-8042
J. Gallagher https://orcid.org/0000-0001-8608-0408
E. Ganster https://orcid.org/0000-0003-4393-6944
A. Garcia https://orcid.org/0000-0002-8186-2459
E. Genton https://orcid.org/0009-0003-5263-972X
A. Ghadimi https://orcid.org/0000-0002-6350-6485
T. Glüsenkamp https://orcid.org/0000-0002-2268-9297
S. J. Gray https://orcid.org/0000-0003-2907-8306
S. Griffin https://orcid.org/0000-0002-0779-9623
S. Griswold https://orcid.org/0000-0002-7321-7513
K. M. Groth https://orcid.org/0000-0002-1581-9049
D. Guevel https://orcid.org/0000-0002-0870-2328
C. Günther https://orcid.org/0009-0007-5644-8559
P. Gutjahr https://orcid.org/0000-0001-7980-7285
C. Ha https://orcid.org/0000-0002-9598-8589
C. Haack https://orcid.org/0000-0003-3932-2448
A. Hallgren https://orcid.org/0000-0001-7751-4489
L. Halve https://orcid.org/0000-0003-2237-6714
F. Halzen https://orcid.org/0000-0001-6224-2417
A. Haungs https://orcid.org/0000-0002-9638-7574
J. Häussler https://orcid.org/0009-0003-5552-4821
K. Helbing https://orcid.org/0000-0003-2072-4172
J. Hellrung https://orcid.org/0009-0006-7300-8961
F. Henningsen https://orcid.org/0000-0002-0680-6588
N. Heyer https://orcid.org/0000-0001-9036-8623
C. Hill https://orcid.org/0000-0003-0647-9174
S. Hori https://orcid.org/0009-0007-2644-5955
M. Hostert https://orcid.org/0000-0002-9584-8877
W. Hou https://orcid.org/0000-0003-3422-7185
T. Huber https://orcid.org/0000-0002-6515-1673
K. Hultqvist https://orcid.org/0000-0003-0602-9472
K. Hymon https://orcid.org/0000-0002-4377-5207
W. Iwakiri https://orcid.org/0000-0002-0207-9010
S. Jain https://orcid.org/0009-0000-7455-782X
O. Janik https://orcid.org/0009-0007-3121-2486
M. Jeong https://orcid.org/0000-0003-2420-6639
M. Jin https://orcid.org/0000-0003-0487-5595
N. Kamp https://orcid.org/0000-0001-9232-259X
D. Kang https://orcid.org/0000-0002-5149-9767
W. Kang https://orcid.org/0000-0003-3980-3778
A. Kappes https://orcid.org/0000-0003-1315-3711
T. Karg https://orcid.org/0000-0003-3251-2126
M. Karl https://orcid.org/0000-0003-2475-8951
A. Karle https://orcid.org/0000-0001-9889-5161
M. Kauer https://orcid.org/0000-0003-1830-9076
J. L. Kelley https://orcid.org/0000-0002-0846-4542
A. Khatee Zathul https://orcid.org/0000-0002-8735-8579
A. Kheirandish https://orcid.org/0000-0001-7074-0539
J. Kiryluk https://orcid.org/0000-0003-0264-3133
S. R. Klein https://orcid.org/0000-0003-2841-6553
Y. Kobayashi https://orcid.org/0009-0005-5680-6614
A. Kochocki https://orcid.org/0000-0003-3782-0128
R. Koirala https://orcid.org/0000-0002-7735-7169
H. Kolanoski https://orcid.org/0000-0003-0435-2524
T. Kontrimas https://orcid.org/0000-0001-8585-0933
C. Kopper https://orcid.org/0000-0001-6288-7637
D. J. Koskinen https://orcid.org/0000-0002-0514-5917
P. Koundal https://orcid.org/0000-0002-5917-5230
M. Kowalski https://orcid.org/0000-0001-8594-8666
A. Kravka https://orcid.org/0009-0003-2120-3130
T. Krishnan https://orcid.org/0000-0002-3237-3114
K. Kruiswijk https://orcid.org/0009-0002-9261-0537
A. Kumar https://orcid.org/0000-0002-8367-8401
N. Kurahashi https://orcid.org/0000-0003-1047-8094
N. Lad https://orcid.org/0000-0001-9302-5140
C. Lagunas Gualda https://orcid.org/0000-0002-9040-7191
M. Lamoureux https://orcid.org/0000-0002-8860-5826
M. J. Larson https://orcid.org/0000-0002-6996-1155
F. Lauber https://orcid.org/0000-0001-5648-5930
J. P. Lazar https://orcid.org/0000-0003-0928-5025
K. Leonard DeHolton https://orcid.org/0000-0002-8795-0601
A. Leszczyńska https://orcid.org/0000-0003-0935-6313
J. Liao https://orcid.org/0009-0008-8086-586X
Q. R. Liu https://orcid.org/0000-0003-3379-6423
Y. T. Liu https://orcid.org/0009-0007-5418-1301
L. Lu https://orcid.org/0000-0003-3175-7770
F. Lucarelli https://orcid.org/0000-0002-9558-8788
W. Luszczak https://orcid.org/0000-0003-3085-0674
Y. Lyu https://orcid.org/0000-0002-2333-4383
J. Madsen https://orcid.org/0000-0003-2415-9959
E. Magnus https://orcid.org/0009-0008-8111-1154

E. Manao https://orcid.org/0009-0002-6197-8574
S. Mancina https://orcid.org/0009-0003-9879-3896
A. Mand https://orcid.org/0009-0005-9697-1702
I. C. Mariş https://orcid.org/0000-0002-5771-1124
S. Marka https://orcid.org/0000-0002-3957-1324
Z. Marka https://orcid.org/0000-0003-1306-5260
I. Martinez-Soler https://orcid.org/0000-0002-0308-3003
R. Maruyama https://orcid.org/0000-0003-2794-512X
J. Mauro https://orcid.org/0009-0005-9324-7970
F. Mayhew https://orcid.org/0000-0001-7609-403X
F. McNally https://orcid.org/0000-0002-0785-2244
K. Meagher https://orcid.org/0000-0003-3967-1533
M. Meier https://orcid.org/0000-0002-9483-9450
L. Merten https://orcid.org/0000-0003-1332-9895
T. Montaruli https://orcid.org/0000-0001-5014-2152
R. W. Moore https://orcid.org/0000-0003-4160-4700
M. Moulai https://orcid.org/0000-0001-7909-5812
T. Mukherjee https://orcid.org/0000-0002-0962-4878
R. Naab https://orcid.org/0000-0003-2512-466X
J. Necker https://orcid.org/0000-0003-0280-7484
L. Neste https://orcid.org/0000-0002-4829-3469
H. Niederhausen https://orcid.org/0000-0002-9566-4904
M. U. Nisa https://orcid.org/0000-0002-6859-3944
K. Noda https://orcid.org/0000-0003-1397-6478
A. Obertacke https://orcid.org/0000-0002-2492-043X
V. O'Dell https://orcid.org/0000-0003-0903-543X
J. Osborn https://orcid.org/0000-0002-2924-0863
E. O'Sullivan https://orcid.org/0000-0003-1882-8802
H. Pandya https://orcid.org/0000-0002-6138-4808
N. Park https://orcid.org/0000-0002-4282-736X
E. N. Paudel https://orcid.org/0000-0001-9276-7994
L. Paul https://orcid.org/0000-0003-4007-2829
C. Pérez de los Heros https://orcid.org/0000-0002-2084-5866
M. Plum https://orcid.org/0000-0001-8691-242X
B. Pries https://orcid.org/0000-0003-4811-9863
L. Pyras https://orcid.org/0000-0003-1146-9659
C. Raab https://orcid.org/0000-0001-9921-2668
N. Rad https://orcid.org/0000-0002-5204-0851
Z. Rechav https://orcid.org/0000-0002-7653-8988
A. Rehman https://orcid.org/0000-0001-7616-5790
E. Resconi https://orcid.org/0000-0003-0705-2770
C. D. Rho https://orcid.org/0000-0002-6524-9769
W. Rhode https://orcid.org/0000-0003-2636-5000
L. Ricca https://orcid.org/0009-0002-1638-0610
B. Riedel https://orcid.org/0000-0002-9524-8943
M. Rongen https://orcid.org/0000-0002-7057-1007
A. Rosted https://orcid.org/0000-0003-2410-400X
C. Rott https://orcid.org/0000-0002-6958-6033
T. Ruhe https://orcid.org/0000-0002-4080-9563
J. Saffer https://orcid.org/0000-0002-0040-6129
D. Salazar-Gallegos https://orcid.org/0000-0002-9312-9684
A. Sandrock https://orcid.org/0000-0002-6779-1172
G. Sanger-Johnson https://orcid.org/0000-0002-4463-2902
M. Santander https://orcid.org/0000-0001-7297-8217
S. Sarkar https://orcid.org/0000-0002-3542-858X
H. Schieler https://orcid.org/0000-0002-2637-4778
S. Schindler https://orcid.org/0000-0001-5507-8890
L. Schlickmann https://orcid.org/0000-0002-9746-6872
F. Schlüter https://orcid.org/0000-0002-5545-4363
F. G. Schröder https://orcid.org/0000-0001-8495-7210
L. Schumacher https://orcid.org/0000-0001-8945-6722
S. Sclafani https://orcid.org/0000-0001-9446-1219
L. Seen https://orcid.org/0009-0004-9204-0241
M. Seikh https://orcid.org/0000-0002-4464-7354
S. Seunarine https://orcid.org/0000-0003-3272-6896
P. A. Sevle Myhr https://orcid.org/0009-0005-9103-4410
R. Shah https://orcid.org/0000-0003-2829-1260
N. Shimizu https://orcid.org/0000-0001-6857-1772
B. Skrzypek https://orcid.org/0000-0002-0910-1057
D. Soldin https://orcid.org/0000-0003-3005-7879
P. Soldin https://orcid.org/0000-0003-1761-2495
G. Sommani https://orcid.org/0000-0002-0094-826X
G. M. Spiczak https://orcid.org/0000-0002-0030-0519
C. Spiering https://orcid.org/0000-0001-7372-0074
J. Stachurska https://orcid.org/0000-0002-0238-5608
T. Stezelberger https://orcid.org/0000-0003-2676-9574
T. Stuttard https://orcid.org/0000-0001-7944-279X
G. W. Sullivan https://orcid.org/0000-0002-2585-2352
I. Taboada https://orcid.org/0000-0003-3509-3457
S. Ter-Antonyan https://orcid.org/0000-0002-5788-1369
M. Thiesmeyer https://orcid.org/0009-0003-0005-4762
W. G. Thompson https://orcid.org/0000-0003-2988-7998
J. Thwaites https://orcid.org/0000-0001-9179-3760
K. Tollefson https://orcid.org/0000-0001-9725-1479
S. Toscano https://orcid.org/0000-0002-1860-2240
A. K. Upadhyay https://orcid.org/0000-0003-1957-2626
A. Vaidyanathan https://orcid.org/0000-0001-6591-3538
N. Valtonen-Mattila https://orcid.org/0000-0002-1830-098X
J. Valverde https://orcid.org/0000-0002-8090-6528
J. Vandenbroucke https://orcid.org/0000-0002-9867-6548
N. van Eijndhoven https://orcid.org/0000-0001-5558-3328
J. van Santen https://orcid.org/0000-0002-2412-9728
S. Verpoest https://orcid.org/0000-0002-3031-3206
J. Villarreal https://orcid.org/0000-0001-9690-1310
A. Wang https://orcid.org/0009-0006-9420-2667
E. H. S. Warrick https://orcid.org/0009-0006-3975-1006
C. Weaver https://orcid.org/0000-0003-2385-2559
A. Y. Wen https://orcid.org/0009-0009-4869-7867
C. Wendt https://orcid.org/0000-0001-8076-8877
N. Whitehorn https://orcid.org/0000-0002-3157-0407
C. H. Wiebusch https://orcid.org/0000-0002-6418-3008
L. Witthaus https://orcid.org/0009-0000-0666-3671
M. Wolf https://orcid.org/0000-0001-9991-3923
J. P. Yanez https://orcid.org/0000-0002-5373-2569
Y. Yao https://orcid.org/0000-0002-4611-0075
S. Yoshida https://orcid.org/0000-0003-2480-5105
F. Yu https://orcid.org/0000-0002-5775-2452
S. Yu https://orcid.org/0000-0003-0035-7766
T. Yuan https://orcid.org/0000-0002-7041-5872
A. Zegarelli https://orcid.org/0000-0003-1497-3826
S. Zhang https://orcid.org/0000-0002-2967-790X
P. Zhelnin https://orcid.org/0000-0003-1019-8375

References

Aartsen, M. G., Ackermann, M., Adams, J., et al. 2017, JInst, 12, P03012
Aartsen, M. G., Abbasi, R., Abdou, Y., et al. 2013, Sci, 342, 1242856
Aartsen, M. G., Abraham, K., Ackermann, M., et al. 2015, PhRvL, 115, 081102
Aartsen, M. G., Ackermann, M., Adams, J., et al. 2018a, Sci, 361, 147
Aartsen, M. G., Ackermann, M., Adams, J., et al. 2019, PhRvD, 99, 032004
Aartsen, M. G., Ackermann, M., Adams, J., et al. 2020a, PhRvL, 125, 121104

Aartsen, M. G., Ackermann, M., Adams, J., et al. 2020b, JCAP, 2020, 042
Aartsen, M. G., Ackermann, M., Adams, J., et al. 2018b, Sci, 361, eaat1378
Abbasi, R., Abdou, Y., Abu-Zayyad, T., et al. 2010, NIMPA, 618, 139
Abbasi, R., Ackermann, M., Adams, J., et al. 2021, PhRvD, 104, 022002
Abbasi, R., Ackermann, M., Adams, J., et al. 2022a, ApJ, 928, 50
Abbasi, R., Ackermann, M., Adams, J., et al. 2022b, Sci, 378, 538
Abbasi, R., Ackermann, M., Adams, J., et al. 2023, Sci, 380, 1338
Abbasi, R., Ackermann, M., Adams, J., et al. 2024, PhRvD, 110, 022001
Ackermann, M., Ajello, M., Baldini, L., et al. 2018, PhRvL, 121, 241101
Aghanim, N., Akrami, Y., Ashdown, M., et al. 2020, A&A, 641, A8
Bilicki, M., Jarrett, T. H., Peacock, J. A., Cluver, M. E., & Steward, L. 2013, ApJS, 210, 9
Bilicki, M., Peacock, J. A., Jarrett, T. H., et al. 2016, ApJS, 225, 5
Chisari, N. E., Alonso, D., Krause, E., et al. 2019, ApJS, 242, 2
Driver, S. P., Bellstedt, S., Robotham, A. S. G., et al. 2022, MNRAS, 513, 439
Fang, K., Banerjee, A., Charles, E., & Omori, Y. 2020, ApJ, 894, 112
Górski, K. M., Hivon, E., Banday, A. J., et al. 2005, ApJ, 622, 759
Hanson, K., & Tarasova, O. 2006, NIMPA, 567, 214
Kaiser, N. 1984, ApJ, 284, L9
Kovács, A., & Szapudi, I. 2015, MNRAS, 448, 1305
Madau, P., & Dickinson, M. 2014, ARA&A, 52, 415
Mainzer, A., Grav, T., Bauer, J., et al. 2011, ApJ, 743, 156
Negro, M., Crnogorčević, M., Burns, E., et al. 2023, ApJ, 951, 83
Ouellette, A., & Holder, G. 2024, PhRvD, 110, 103025
Paopiamsap, A., Alonso, D., Bartlett, D. J., & Bilicki, M. 2024, PhRvD, 109, 103517
Peebles, P. J. E. 1980, The Large-scale Structure of the Universe (Princeton Univ. Press)
Schlafly, E. F., Meisner, A. M., & Green, G. M. 2019, ApJS, 240, 30
Schlegel, D. J., Finkbeiner, D. P., & Davis, M. 1998, ApJ, 500, 525
Skrutskie, M. F., et al. 2006, AJ, 131, 1163
Tung, C. F., Glauch, T., Larson, M., et al. 2021, JOSS, 6, 3194
Wright, E. L., Eisenhardt, P. R. M., Mainzer, A. K., et al. 2010, AJ, 140, 1868
Zhang, P., & Beacom, J. F. 2004, ApJ, 614, 37